

Twin spin/charge roton mode and superfluid density: primary determining factors of T_c in high- T_c superconductors observed by neutron, ARPES, and μ SR

Y. J. Uemura

Physics Department, Columbia University, 538 West, 120th Street, New York, NY 10027, USA

Abstract

In the quest for primary factors which determine the transition temperature T_c of high- T_c cuprate superconductors (HTSC), we develop a phenomenological picture combining experimental results from muon spin relaxation (μ SR), neutron and Raman scattering, and angle-resolved photoemission (ARPES) measurements, guided by an analogy with superfluid ^4He . The 41 meV neutron resonance mode and the ARPES superconducting coherence peak (SCP) can be viewed as direct observations of spin and charge soft modes, respectively, appearing near (π, π) and the center of the Brillouin zone, having identical energy transfers and dispersion relations. We present a conjecture that the mode energy of this twin spin/charge collective excitation, as a roton analogue in HTSC, plays a primary role in determining T_c , together with the superfluid density n_s/m^* at $T \rightarrow 0$. We further propose a microscopic model for pairing based on a resonant spin-charge motion, which explains the extremely strong spin-charge coupling, relevant energy scales, disappearance of pairing in the overdoped region, and the contrasting spin-sensitivities of nodal and antinodal charges in HTSC systems. Comparing collective versus single-particle excitations, pair formation versus condensation, and local versus long-range phase coherence, we argue that many fundamental features of HTSC systems, including the region of the Nernst effect, can be understood in terms of condensation and fluctuation phenomena of bosonic correlations formed above T_c .

Key words: high- T_c superconductivity, μ SR, ARPES, neutron scattering.

1. Introduction

Since the author joined the research group of Prof. Toshimitsu Yamazaki at the Univ. of Tokyo in 1976, the ultimate goal of our research has been to combine powerful modern experimental techniques with insightful physics phenomenology. In

this lecture, we would like to present our attempt towards this goal in 18 years of study on high- T_c cuprate superconductors (HTSC), motivated by the quest for primary factors which determine T_c , and guided by an instructive analogy between HTSC and superfluid He systems. Some seed ideas of the present work have been discussed in ref. [1].

* Tel. +1 212 854 8370, Fax: +1 212 854 3379, email: tomo@lorentz.phys.columbia.edu

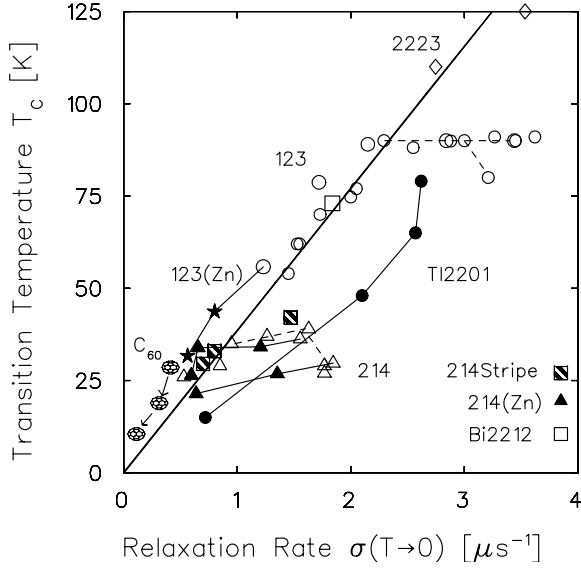


Fig. 1. Muon spin relaxation rate $\sigma \propto n_s/m^*$ at $T \rightarrow 0$ from various high- T_c cuprate superconductors [2,1] and A_3C_{60} systems plotted against the superconducting transition temperature T_c . The points for HTSC with open symbols represent simple hole doped systems, while closed triangles are for (Cu,Zn) substitution [3], “stripe” symbols for systems with formation of island regions with incommensurate static spin modulations [4], and closed circles for overdoped TI2201 [5].

2. Superfluid Energy Scales vs. T_c

By 1989, within a few years after the discovery of HTSC systems, we established [1,2] strong correlations between T_c and n_s/m^* (superconducting carrier density / effective mass) at $T \rightarrow 0$ by measuring the muon spin relaxation rate σ and the London penetration depth λ as $\sigma \propto 1/\lambda^2 \propto n_s/m^*$. As shown in Fig. 1, a nearly linear relationship between T_c and n_s/m^* (often referred to as the “superfluid density”) holds in most of the underdoped cuprates as well as in HTSC systems with Cu/Zn substitutions [3], formation of island regions having static stripe spin correlations [4], and overdoped systems having microscopic phase separation between superfluid and normal unpaired fermions [5,6]. The strong correlation was one of the earliest signatures suggesting fundamental difference of HTSC systems from BCS superconductors. The robustness of this relationship against heterogeneity, analogous to the case in superfluid

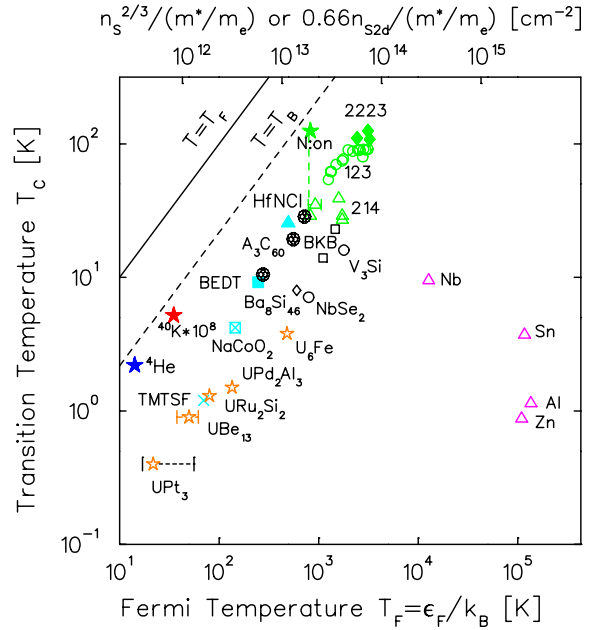


Fig. 2. (color) Plot of T_c versus the effective Fermi temperature T_F obtained from the superfluid response n_s/m^* of various superconducting systems, first attempted in ref. [7] in 1991, and updated [1]. We see an empirical upperlimit $T_c/T_F \sim 0.05$ for superconducting systems. Also included are the corresponding points for the superfluid ^4He (blue star). The T_B line shows the BE condensation temperature for the ideal Bose gas of boson density $n_s/2$ and mass $2m^*$. The green star represents the onset temperature T_{on} of the Nernst effect, shown in Fig. 12, for $\text{La}_{1.9}\text{Sr}_{0.1}\text{CuO}_4$ [29].

He films and $^3\text{He}/^4\text{He}$ mixture films on regular and porous media [1], can be expected only for systems with very strong coupling. In Fig. 1, we also notice that the 214 systems exhibit an “early branching off” from the nearly linear relationship, which we will ascribe to the closeness to competing magnetic states, as discussed later.

In 1991 [7], we converted the superfluid density into the effective Fermi temperature T_F , which represents an effective kinetic energy scale of mobile superconducting carriers corresponding to the “Drude” spectral weight in optical responses. The results in Fig. 2 are shown together with the Bose-Einstein (BE) condensation temperature T_B expected when all the superconducting carriers form a non-interacting ideal Bose gas with the density $n_s/2$ and mass $2m^*$. The transition temperatures T_c of HTSC, organic BEDT, and some other novel

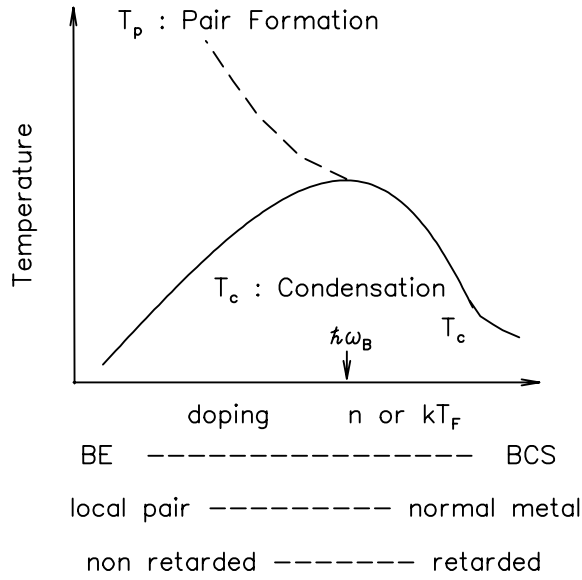


Fig. 3. The BE-BCS crossover picture proposed by Uemura [8,9] in 1994 with the crossover region characterized by the matching of kinetic energy $k_B T_F$ of the condensing carriers with the mediating boson energy $\hbar\omega_B$. When one identifies the pair formation temperature T_p as the pseudo-gap temperature T^* , this phase diagram can be mapped to the case of HTSC.

superconductors are reduced by a factor 4-5 from T_B , while the above-mentioned linear relationship emerges to be parallel to the T_B line. This feature suggests a fundamental importance of the BE condensation concept in cuprates. The blue star point represents the superfluid transition of (3-dimensional) liquid He, at $T_\lambda = 2.2$ K which is about 50 % reduced from the $T_B = 3.2$ K calculated with the number density and mass. Figure 2 can be viewed as an experimentalist's way to classify various superconductors and superfluids between the two extrema of idealized BE and BCS condensations in the strong and weak-coupling limits.

3. BE-BCS crossover and phase diagram of HTSC

In 1993-94 we proposed a conjecture [8-10] that the phase diagram of HTSC systems can be mapped onto a general concept of BE to BCS

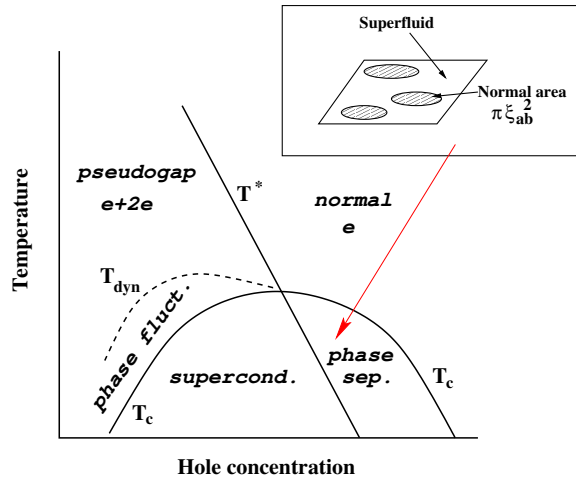


Fig. 4. (color) A generic phase diagram proposed for cuprates by Uemura [1,12], including the distinction between the pair formation T^* and the onset temperature of dynamic superconductivity T_{dyn} which corresponds to the T_{on} of the Nernst effect in Fig. 12. Dynamic superconductivity is associated with phase fluctuations of bosonic wavefunctions. The inset illustrates the microscopic phase separation between superconducting and normal metal regions in the overdoped region [6].

crossover shown in Fig. 3. When bosonic correlations develop well above T_c , BE condensation occurs when the thermal wave length of bosons becomes comparable to the interboson distance, resulting in $T_c \propto n_s/m^*$ in 2-d and $n_s^{2/3}/m^*$ in 3-d systems. In the BCS condensation, the attractive “pairing” energy scale (i.e., the gap) determines T_c , since the number-density restriction for BE condensation is readily satisfied when the Cooper pairs (bosons) are formed at T_c . The T_c v.s. n_s/m^* correlations and the pseudogap behavior lead to a view that the underdoped cuprates are in the BE region, with the T^* representing pair (boson) formation above T_c . In this mapping, the optimal-doping region lies in the crossover region, where the number-density energy scale (the effective Fermi temperature T_F) is close to the energy of pair mediating interaction $\hbar\omega_B$. In HTSC systems, the optimum region appears around $T_F \sim 2000$ K. Hence the antiferromagnetic spin fluctuations, having a similar energy scale, become an attractive candidate for the pairing mediator [10].

Figure 4 shows our current view of the actual HTSC phase diagram [1,12]. Several experimen-

tal results [5-6] in the overdoped region indicate existence of microscopic phase separation, as we first suggested in 1993 [5] and as has been directly confirmed very recently by scanning tunneling microscopy (STM) studies [11]. The overdoped region is thus quite different from the simple BCS situation. When the pairing strength T^* rapidly decreases with increasing doping (increasing T_F), the system responds by creating a “phantom superconducting” region where superconductivity is maintained by microscopic phase separation to gain condensation energy at the expense of Coulomb energy for charge disproportionation [6].

4. Collective soft-mode energies determining T_c

In superfluid 3-d liquid ^4He , the reduction of the lambda temperature $T_\lambda = 2.2$ K from the idealized $T_B = 3.2$ K is caused by the existence of roton excitation, which is a soft phonon mode towards solidification of He. Figure 5(a) shows the phonon-roton dispersion relation [13] together with the Bragg peaks of solid He [14]. The effect of roton on T_c can be clearly seen via the nearly linear relationship in Fig. 6 which plots $T_\lambda = T_c$ versus the roton mode energy (observed at different pressures [15]: orange-star symbols), where the He values for the both axes are multiplied by a factor 60 to be compared with the cuprates. Helium rotons demonstrate that the closeness to the competing state (solid He) influences the condensation temperature of a bosonic superfluid.

Guided by an analogy to He, we plot the energy of the 41 meV magnetic resonance mode of HTSC [16] versus T_c in Fig. 6. Also plotted is the energy of A_{1g} Raman mode which follows the same relationship [17]. The magnetic resonance mode is a soft-magnon mode towards the magnetically ordered stripe state competing with the superconducting state, analogous to He rotons being a soft phonon mode towards a competing state. The neutron resonance detects an $S=1$ excitation with the wavevector transfer (π, π) , while the Raman mode represents an $S=0$ excitation near the zone center. In most of known cases, the “2-magnon” mode in

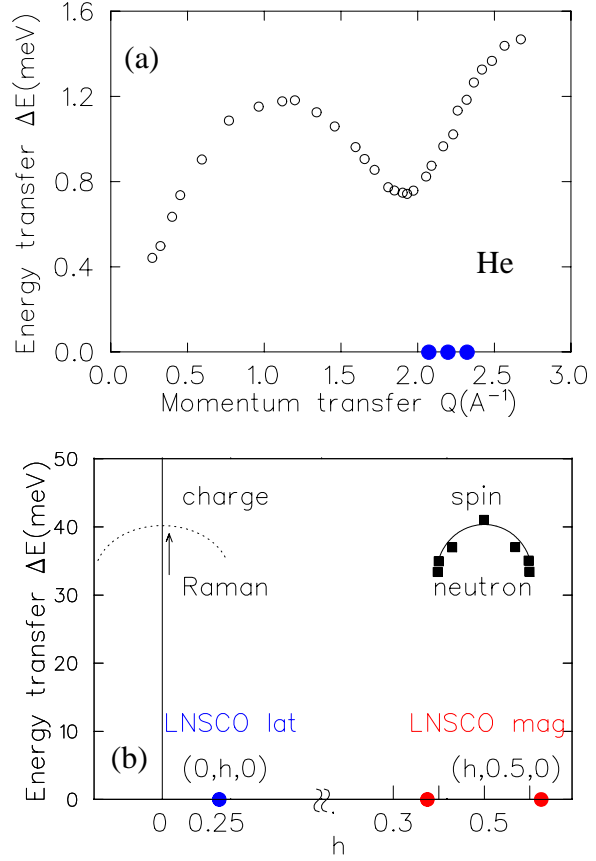


Fig. 5. (color) (a) The dispersion relation of phonon-roton excitations in superfluid ^4He observed by neutron scattering [13]. The closed circles show the Bragg points of HCP solid He [14] at the pressure of 66 atmospheres at $T = 1.1$ K. (b) The dispersion relation around the (π, π) resonance mode observed in YBCO by neutrons [16] (closed squares), the location of the satellite Bragg peaks (red = magnetic; blue = lattice, estimated from the adjacent Brillouin zone) found in the static spin/charge stripe system $(\text{La}, \text{Nd}, \text{Sr})_2\text{CuO}_4$ (LNSCO) [18], and the proposed charge branch of the twin spin/charge roton (dotted line), to which the Raman A_{1g} response and the ARPES SCP in Figs. 6 and 8 are ascribed.

Raman measurements, having twice the magnon energy, is required to match the nearly zero net momentum transfer in Raman measurements. In contrast, Fig. 6 shows a one-to-one correspondence of neutron and Raman energies. This apparent contradiction can be resolved by assuming a roton-analogue twin mode in HTSC [1], having the spin-branch near (π, π) and charge branch near the zone center, with the same energy minimum and disper-

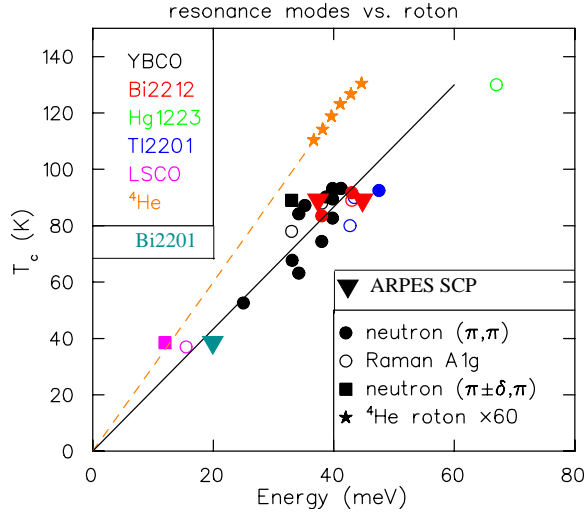


Fig. 6. (color) The plot of T_c versus energy of the roton minimum of bulk superfluid ^4He (values for both axes multiplied by a factor 60) measured under applied pressures [15], compared with the relationship seen in HTSC systems for the energies of the neutron resonance mode at (π, π) [16,1], the Raman A_{1g} mode [17,1], and the ARPES SCP [23]. Also included are the neutron energy transfers of spectral weight maximum near the $(\pi \pm \delta, \pi)$ point in YBCO [16] and LSCO [19] (closed squares).

sion, as illustrated in Fig. 5(b).

Indeed the competing states in the cuprates, such as the stripe state or the Mott insulator antiferromagnetic state, have both spin and charge orders, with the spin Bragg peak (red circles in Fig. 5(b)) and charge Bragg peak (blue circles) appearing when that state wins against the superconducting state [18]. When the superconducting state wins, the spin-charge modulations become dynamic, yet conserving the very strong correlations with each other and having the same soft-mode energy transfers corresponding to the “superconducting condensation energy”. Via this mechanism, although neutrons and photons (in the Raman studies) create different final states ($S=1$ and $S=0$ states) with different momentum transfers, the spin and charge branches appear with the same energy transfers. The magnon soft-mode can exist only when it is associated with the partner dynamic charge modulation. Thus the excitation of the 41 meV mode contributes to the reduction of superfluid density, playing a role similar to He rotons, leading to a linear relationship

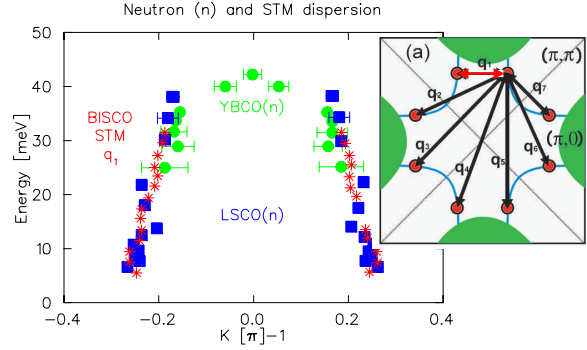


Fig. 7. (color) The dispersion relation of the neutron resonance mode, measured around the momentum transfer (π, π) in YBCO and LSCO [19] systems near optimal doping, compared with the dispersion of the q_1 charge scattering mode measured by the Fourier transform STM spectroscopy in Bi2212 [21]. The momentum transfer for the latter is scaled by a factor 2 to account for the difference between the spin modulation with the $1/8$ periodicity and the charge modulation with the $1/4$ periodicity, connecting the Fermi arcs near the antinodal points $(0, \pi)$. The inset figure shows the Brillouin zone and the STM q_1 mode with the red arrow.

between T_c and the mode energy for HTSC systems as shown in Fig. 6. This analogy between He and HTSC is strengthened by their nearly equal ratios of mode energy and T_c .

5. Common spin-charge dispersion relation and ARPES coherence peak as the charge branch

The 41 meV spin-branch exhibits a dispersion relation, extending downwards towards the satellite stripe Bragg peaks, as shown for $\text{YBa}_2\text{Cu}_3\text{O}_{7-\delta}$ (YBCO) and $\text{La}_{2-x}\text{Sr}_x\text{CuO}_4$ (LSCO) [19] in Fig. 7 and even in non-superconducting $\text{La}_{2-x}\text{Ba}_x\text{CuO}_4$ (LBCO) with $x = 1/8$ [20]. There seem to be two cases: (a) the mode energy at (π, π) is reduced for systems with lower T_c 's, such as in the underdoped YBCO; and (b) the dispersion itself does not change but the lower-energy branch is populated for systems with lower T_c 's, such as in LSCO and LBCO 214 cuprates. When we plot the energy of the spectral-weight maximum of the lower-energy populated branch, which is often referred to as the “spin gap energy” in neutron studies,

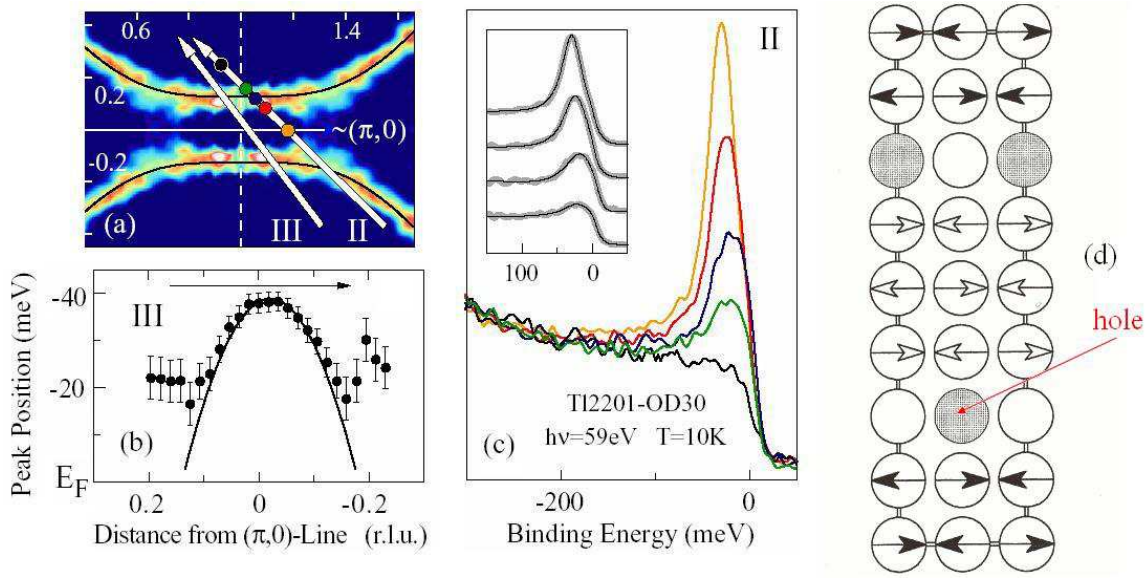


Fig. 8. (color) The ARPES superconducting coherence peak (SCP) observed in overdoped $\text{Tl}_2\text{Ba}_2\text{CuO}_{6+\delta}$ (Tl2201) with $T_c = 30\text{ K}$ [22]. (a) The trajectory of momentum in the reciprocal space near the antinodal point $(\pi, 0)$. (b) The dispersion relation observed along the line III in (a), which is nearly identical to those shown in Fig. 7. Note that the peak position energy, multiplied by (-1), corresponds to the energy input given by the ARPES photon to the system. (c) The intensity versus energy profile of the SCP measured along the line II in (a). (d) Real-space pattern of the stripe spin-charge modulations in the cuprates [18]. Doped holes reside with Cu atoms shown by the shaded area, which have neighbouring Cu spins with opposite directions. This leads to the “geometrical frustration” for the spin of a charge liberated in ARPES from the dynamic stripe spin-charge correlations.

the correspondence with superfluid He becomes even better, as shown by the filled square symbols in Fig. 6. Christesen *et al.* [19] noticed that, after a factor 2 adjustment of momentum transfers, the same dispersion relation is also seen in the q_1 charge scattering observed in the STM studies in $\text{Bi}_2\text{Sr}_2\text{CaCu}_2\text{O}_{8+\delta}$ (Bi2212) [21], shown by the red star symbols in Fig. 7.

The present author has recently noticed that this “common dispersion of spin and charge responses” appears also in the ARPES results of the “superconducting coherence peak” (SCP), obtained by Platé *et al.* [22] in Tl2201 near the antinodal wavevector $(\pi, 0)$. Figure 8 shows the energy-transfer by photons to the system in ARPES (i.e., negative peak energy) plotted versus the distance of the momentum transfer from $(\pi, 0)$, showing dispersion nearly identical to those in Fig. 7. Furthermore, the energy transfer of the ARPES SCP [23] closely follows the relationship found for neutron and Raman modes, as shown in Fig. 6 with

filled-triangle symbols. These observations suggest that the ARPES SCP may be interpreted as a direct manifestation of the charge branch of the twin spin-charge soft mode.

6. Collective mode versus single-particle pair-breaking excitations

Although fundamental differences of HTSC from traditional BCS superconductors were noticed by the mid 1990’s, the destruction of superfluid density has almost always been discussed exclusively in terms of single-particle pair-breaking excitations: people’s minds have still been controlled by the BCS theory. This tendency has perhaps been enhanced by the successful explanation of the low-temperature penetration depth results by the d-wave nodal quasiparticle excitations.

Single-particle excitations would cost the gap energy $\Delta(k)$ in pair breaking. Imagine a spin-singlet

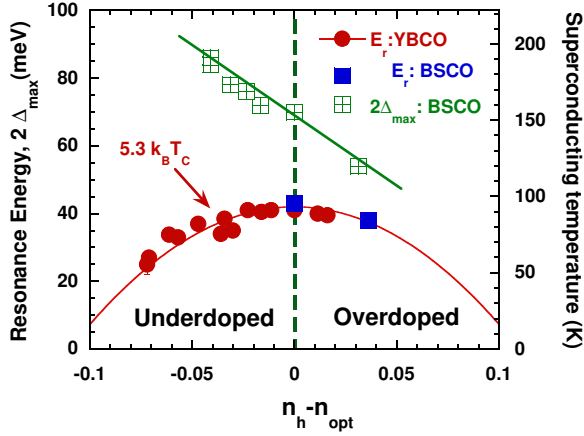


Fig. 9. (color) Doping dependence of the resonance mode energy determined by neutron scattering [16] compared to the gap energy 2Δ determined by tunneling measurements in HTSC systems. The mode energy scales with T_c in the whole doping range, but the gap shows the doping dependence opposite to that of T_c in the underdoped region.

charge pair formed to gain the antiferromagnetic exchange energy J . Input of energy J is required to flip the spin in the single-particle process. In collective excitations based on many-body correlations, a spin triplet excitation can be realized as a spin wave which can be obtained without an energy input of J . This is why the $S=1$ neutron resonance mode does not cost any pair-breaking energy. Indeed, the mode energy in the underdoped HTSC, proportional to T_c , follows the doping dependence completely opposite to the behavior of the gap (and pairing) energy Δ (and T^*), as illustrated in Fig. 9 [16]. It is very difficult to ascribe T_c to the nodal quasiparticle pair-breaking excitations [24], in view of this opposite behavior of Δ and T_c .

From a single-particle type view, an ARPES excitation near the antinodal $(\pi, 0)$ point requires to break the Cooper pair, costing the gap energy Δ , in addition to any bosonic mode energy Ω to which the charge is coupled. So, the SCP energy has been discussed in terms of $\Delta + \Omega$ [25]. However, imagine the case when the energy input by ARPES photon is used to create collective dynamic spin-charge modulations, as illustrated in Fig. 8(d) [18]. Thanks to the microscopic separation of spins and charges in this stripe pattern, the spin of a hole is

“frustrated” with the neighbouring Cu moments. This “geometrical frustration” makes the spin direction of the charge irrelevant when the charge is knocked out as the ARPES photo-electron: the charge liberation does not cost the pairing energy J or Δ . Therefore, we would expect direct correspondence of the ARPES SCP energy to the boson mode energy Ω for the case of collective excitations of the charge soft mode. This explains the agreement of neutron and SCP energies in Fig. 6. Such a liberated charge would carry momentum of the “broken” charge-density-wave pair correlation, as clearly seen from the ARPES momentum in Fig. 8(a) [22].

7. Microscopic pairing via resonant spin-charge motion

These considerations suggest that pairing in HTSC should involve: (1) a very strong spin and charge coupling; (2) energy scale of T_F (charge kinetic energy) comparable to that of pair-mediation interaction; and (3) disappearance of pairing in the overdoped region. Guided by these, the present author proposed a pairing mechanism in 2004 [1] based on resonant spin-charge motion of antinodal charges.

Figure 10 shows a motion of a hole in dynamic antiferromagnetic (AF) correlations of surrounding Cu moments. When the AF pattern is static, a charge motion towards the Cu-O bond direction (with the antinodal momentum) would cause three frustrated bonds (Fig. 10(a)). However, when this charge motion occurs in sequence with half a period of AF fluctuations, frustrations can be avoided (Fig. 10(b)). Within one period, the charge would proceed twice the lattice constant a . This process brings a very strong coupling between the AF fluctuations with $\hbar\omega_{AF}$ and the antinodal charges at the zone boundary with $k = 2\pi/2a$ having the Fermi energy $kT_F = \hbar\omega_{AF}$. Only when accompanied by a resonant AF fluctuation can an antinodal charge move freely in the system.

Thus, antinodal charge motion should always be associated with an AF spin fluctuation, similarly to the charge motion in BCS superconductors as-

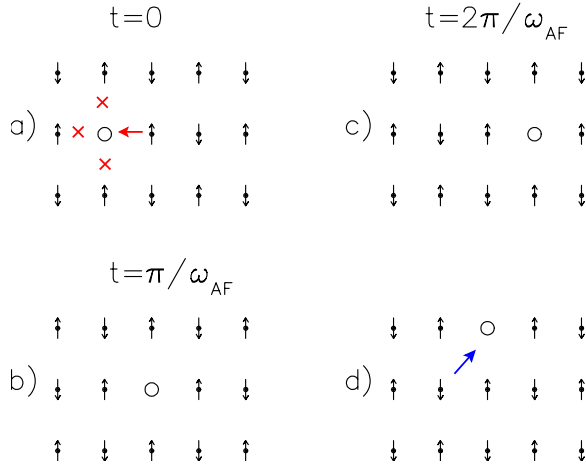


Fig. 10. (color) An illustration of a charge motion in the cuprate resonant with the antiferromagnetic spin fluctuations with the frequency ω_{AF} . (a) shows the $t = 0$ configuration, and the three frustrated bonds created when the charge hops while the surrounding spins keep their directions. (b) shows the case in which a charge hops at $t = \pi/\omega_{AF}$ after a half period when surrounding spins have changed their directions. (c) shows the situation after the full period $t = 2\pi/\omega_{AF}$ for the propagation towards the $(\pi, 0)$ direction, representing the case for an antinodal charge with wavevector $k = 2\pi/2a$ having $kT_F = \hbar\omega_{AF}$. Spin frustration can be avoided via the dynamical motion in (b) and (c). (d) shows that the diagonal motion of a nodal charge on the same spin sublattice does not create frustrated bonds regardless of the time sequence of motion with respect to the AF spin fluctuations.

sociated with lattice deformation, i.e., a phonon. The existence of a AF fluctuation can provide an energy benefit to the second antinodal charge. This results in a “scattering” process which couples antinodal charges with opposite momentum, as shown in Fig. 11(a). Unlike BCS, however, this coupling is not retarded. This process would create a substantial attractive interaction among antinodal charges, which would lead to the opening of the “pseudo gap” [1].

As the energy scale kT_F is much higher than the mode energy of roton-analogue spin-charge modulations, the AF fluctuations in the above mentioned process are mostly high energy fluctuations near (π, π) well above the soft-mode energy. The resonant process would couple such high energy spin fluctuations with the partner charge fluctuation/motion near the zone center, having compa-

table energies. Increasing charge doping in HTSC would increase this charge energy scale kT_F . When kT_F exceeds the spin energy scale J , as presumably happening in the overdoped region, the resonant coupling mechanism is lost. Charge doping in cuprates also weakens spin correlations via introduction of frustration. These features explain the loss of pairing, followed by emergence of “phantom superconductivity” in the overdoped region.

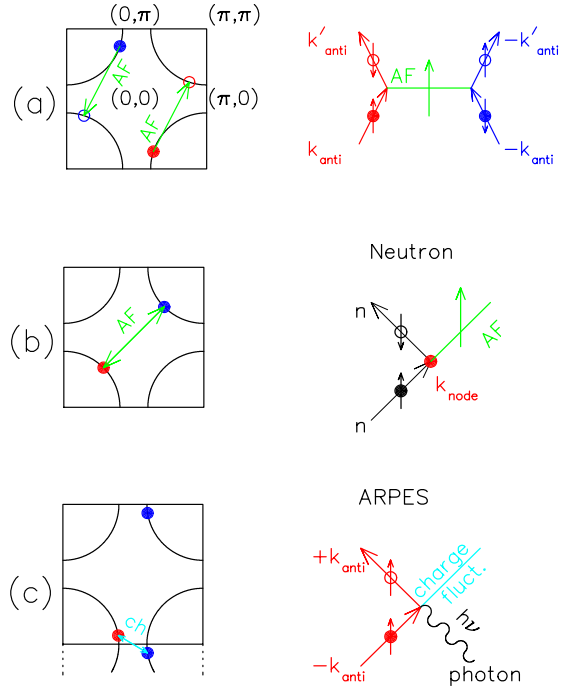


Fig. 11. (color) (a) An illustration of the attractive interaction obtained in the scattering process of AF spin fluctuations by antinodal charges, which leads to the opening of the pseudogap. (b) and (c) illustrate that the spin and charge soft modes, respectively, can be viewed as Yakawa-type bonding bosons, with the “vacuum” corresponding to the situation having dynamic stripe spin-charge modulations. The energy and momentum input by neutrons to nodal charges liberate an AF spin fluctuation to this “vacuum equivalent”, leading to the resonance mode, while energy input of ARPES photon liberates the charge fluctuations (by breaking the charge-density wave pair formed by antinodal charges), leading to the ARPES SCP. These liberation processes occur at a cost of condensation energy, corresponding to the twin spin/charge roton energy, with the intensities proportional to the superfluid density n_s/m^* .

8. Difference between nodal and antinodal charges

In contrast to antinodal charges, nodal charges are moving on the same spin sublattice, as shown in Fig. 10(d). Therefore, nodal charges are not subject to spin frustration, regardless of how their energies compare with energies of AF fluctuations. This fundamental difference between the “spin-sensitive” antinodal and “spin-insensitive” nodal charges would explain why the ARPES Fermi-energy spectral weight [26] resides mainly in the nodal region in the underdoped cuprates having strong AF fluctuations. The antinodal charges dominate ARPES response in the overdoped region where AF correlations die away, and where the antinodal charges become “spin-insensitive”.

If one tries to show the spin and charge roton-like modes in a single-particle diagram of Fig. 11(b) and (c), the spin mode appears as connecting two nodal charges and the charge mode connecting two antinodal charges, analogous to nucleon binding via a Yukawa meson. In these diagrams, “vacuum” corresponds to the situation with dynamic spin/charge stripe correlations. Neutron scattering then liberates the $S=1$ AF magnon, while ARPES liberates the charge fluctuation, into such a “vacuum equivalent”, with the energy input corresponding to the condensation energy, as shown in Fig. 11(b) and (c). The intensity of these liberation processes should be proportional to the superfluid density, as was actually observed in neutron and ARPES measurements [16,23].

9. Phase fluctuations, roton-like excitations, and Nernst region

In purely 2-d systems, such as a thin film of superfluid He on regular or porous media, superfluidity is destroyed via liberation of vortex-antivortex pair at the Kosterlitz-Thouless (KT) transition temperature T_{KT} , where the superfluid density n_s/m^* at $T = T_{KT}$ follows the system-independent universal value given by the KT theory [27]. Since the roton energy scale is much higher than T_{KT} , the 2-d superfluid density in typ-

ical He films shows little temperature dependence at $0 < T < T_{KT}$, as shown in Fig. 5(a) of ref. [1]. In He thin-films, “dynamic superfluidity” with dissociated vortices exists at $T_{KT} < T < T_{BE} = 3.2$ K, as can be seen in the specific heat results.

In cuprate systems, with increasing temperature, the superfluid density is destroyed by the nodal pair-breaking excitations at low temperatures up to $T \sim T_c/2$, presumably followed by the reduction due primarily to excitations of the twin spin-charge soft mode at $T_c/2 < T < T_c$. For the case of highly 2-d cuprates, such as Bi2212, the system undergoes the KT transition with sufficiently reduced superfluid density at T_c [28]. In systems close to the magnetic states, such as the 214 systems near the 1/8 doping concentration, T_c is determined by the soft mode energy, i.e., the closeness to the competing state. In either types of cuprates, the normal state above T_c exhibits “dynamic superconductivity”, as was demonstrated by the observation of Nernst effect [29] shown in Fig. 12.

For bosonic systems where the pairing energy

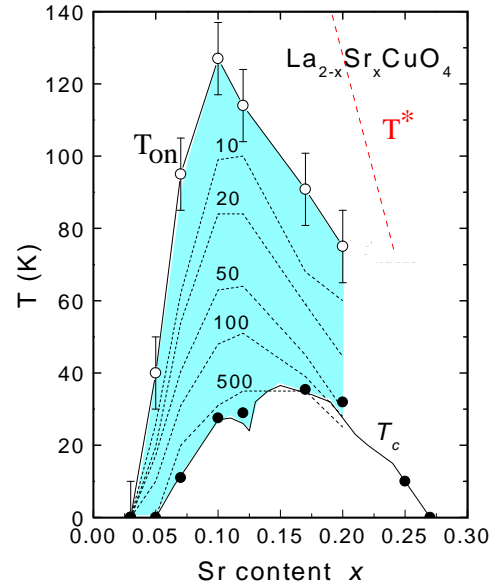


Fig. 12. (color) The region of the Nernst effect, shown in the T - x phase diagram for $\text{La}_{2-x}\text{Sr}_x\text{CuO}_4$ (LSCO) [29]. The on-set temperature of the Nernst effect is denoted by T_{on} . The result of T_{on} for the $x = 0.10$ sample is plotted with the green star symbol in Fig. 2. The value of T^* was taken from [30].

scale T^* is higher than the number-density scale T_B , we expect the Nernst region to extend up to T_B . Indeed, the Nernst on-set temperature $T_{on} \sim 130$ K of 10% Sr doped LSCO system [29] (green star) lies very close to the T_B line in Fig. 2 [1], and T_{on} increases with increasing doping in the very underdoped region in Fig. 12, following the behavior of T_B . The reduction of T_{on} near the optimum doping region in Fig. 12 can be explained by the reduction of T^* , which makes bosons unavailable. Thus, the Nernst effect occurs with two conditions: (1) availability of bosons, i.e., $T < T^*$; and (2) sufficient number density of bosons to build up local phase coherence, i.e. $T < T_B$. The Nernst region above T_c can be characterized by the existence of bosonic amplitude without static long-range phase coherence. If it were possible to remove factors which destroy long-range phase coherence, such as the soft mode and low dimensionality, cuprate systems would have acquired superconductivity at the Nernst onset temperature T_{on} .

Since the soft-mode energy is related to condensation energy, superfluid density influences the mode energy. However, due to relevance of competing states, n_s/m^* at $T \rightarrow 0$ is no longer a sole factor in determining T_c . This feature is clearly seen for the case of 214 cuprates, which are particularly close to the competing magnetic state, having lower soft-mode energies, thus showing earlier branching off from the linear relationship in Fig. 1, compared to YBCO systems with comparable values of $\sigma(T \rightarrow 0) \propto n_s/m^*$. In this way, superfluid density and the soft-mode energy “conspire or cooperate” in determining T_c . Further studies of microscopic pairing mechanisms and collective modes would hopefully clarify the origin of apparently universal upperlimit of $T_c/T_B \sim 1/4$ common to various correlated electron superconductors shown in Fig. 2.

This work has been supported by the NSF DMR-0102752, DMR-0502706, INT-0314058 and CHE-0111752 (Nanoscale Science and Engineering Initiative). The author thanks J.C. Davis, A. Damascelli, N. Nagaosa for useful discussions; G.M. Luke and S. Uchida for continuing collaboration; and T. Yamazaki for excellent guidance in the beginning of the author’s scientific career.

References

- [1] Y.J. Uemura, J. Phys. Condens. Matter **16** (2004) S4515.
- [2] Y.J. Uemura *et al.*, Phys. Rev. Lett. **62** (1989) 2317.
- [3] B. Nachumi *et al.*, Phys. Rev. Lett. **77** (1996) 5421.
- [4] K.M. Kojima *et al.*, Physica **B 36** (2003) 316.
- [5] Y.J. Uemura *et al.*, Nature (London) **364** (1993) 605.
- [6] Y.J. Uemura, Solid State Commun. **120** (2001) 347.
- [7] Y.J. Uemura *et al.*, Phys. Rev. Lett. **66** (1991) 2665.
- [8] Y.J. Uemura, in *Polarons and Bipolarons in High- T_c Superconductors and Related Materials*, ed. by E. Salje, A.S. Alexandrov and Y. Liang, Cambridge University Press (1995), p.p. 453.
- [9] Y.J. Uemura, in Proceedings of International Symposium/Workshop on High- T_c Superconductivity and the C_{60} Family, May 1994, Beijing, ed. by H.C. Ren, Gordon and Breach (New York), (1995), p.p. 113.
- [10] Y.J. Uemura, Physica **C282-287** (1997) 194.
- [11] J.C. Davis, private communications (2005).
- [12] Y.J. Uemura, Solid State Commun. **126** (2003) 23 ; erratum *ibid* 425.
- [13] D.G. Henshaw and A.D.B. Woods, Phys. Rev. **121** (1961) 1266.
- [14] D.G. Henshaw, Phys. Rev. **109** (1958) 328.
- [15] O.W. Dietrich *et al.*, Phys. Rev. **A5** (1972) 1377.
- [16] P. Bourges *et al.*, Physica **C424** (2005) 45.
- [17] Y. Gallais *et al.*, Phys. Rev. Lett. **88** (2002) 177401.
- [18] J.M. Tranquada *et al.*, Nature **375** (1995) 561.
- [19] N.B. Christensen *et al.*, Phys. Rev. Lett. **93** (2004) 147002.
- [20] J.M. Tranquada *et al.*, Nature **429** (2004) 534.
- [21] K. McElroy *et al.*, Nature **422** (2003) 592.
- [22] M. Pláté *et al.*, Phys. Rev. Lett. **95** (2005) 077001.
- [23] A. Damascelli, Z. Hussain, Z.X. Shen, Rev. Mod. Phys. **75** (2003) 473 (see Fig. 50 at p. 513).
- [24] P.A. Lee and X.G. Weng, Phys. Rev. Lett. **78** (1997) 4111.
- [25] M.R. Norman and C. Pepin, Rep. Prog. Phys. **66** (2003) 1547.
- [26] T. Yoshida *et al.*, Phys. Rev. Lett. **91** (2003) 027001.
- [27] J.M. Kosterlitz and D.J. Thouless, J. Phys. **C: Solid State Phys.** **6**, (1973) 1181.
- [28] J. Corson *et al.*, Nature (London) **398** (1999) 221.

- [29] Y. Wang *et al.*, Phys. Rev. **B64** (2001) 224519.
- [30] T. Timusk and B. Statt, Rep. Prog. Phys. **62** (1999) 61.